1-4 Optical Coherence Techniques for Plasma Doppler Spectroscopy

J. Howard, C. Michael, F. Glass and A. D. Cheetham
Plasma Research Laboratory,
Australian National University. Canberra ACT 0200
http://rsphysse.anu.edu.au/prl/MOSS.html

Abstract

A new electro-optically Modulated Optical Solid-State (MOSS) interferometer has been constructed for measurement of the low order spectral moments of line emission from optically thin radiant media. The instrument, which is based on the principle of the Fourier transform spectrometer, has high etendue and is rugged, compact and inexpensive. By employing electro-optical path-length modulation techniques, the spectral information is transferred to the temporal frequency domain and can be obtained using a single photodetector. Specifically, the zeroth moment (brightness) is given by the average signal level, the first moment (shift) by the modulation phase and the second moment (line width) by the modulation amplitude.

1 Introduction

This paper describes an electro-optically modulated solid state (MOSS) spectrometer for general purpose optical plasma spectroscopy [3, 4]. The spectrometer monitors the temporal coherence of an isolated spectral line using polarization interferometric techniques. It is essentially a Fourier transform spectrometer modulated about a fixed delay. The amplitude of the interference fringes produced by the modulation is related to the light temporal coherence while the phase conveys the line centre frequency.

When the line-centre frequency changes (e.g. Doppler drift), the interferogram phase varies (much like an accordion), leaving the envelope unchanged. On the other hand, when the lineshape (e.g. Doppler width) changes, only the coherence envelope is affected, the carrier phase remaining undisturbed. As shown below, this decoupling of first and higher-order spectral moments is one of the more important fundamental advantages offered by time-domain spectroscopic methods applied to spectroscopy of plasmas.

In this paper we discuss a number of experiments based on MOSS technology that are presently installed on the H-1 heliac at the ANU. These include the MOSS spectroscopic camera (see also Michael and Howard - these proceedings), the ToMOSS (Tomographic MOSS) spectroscopy system, the SOFT (Spread-spectrum Optical Fourier Transform) spectrometer and various polarization spectroscopy systems.

2 MOSS spectrometer

The spectrometer is shown in Fig. 1. A narrowband interference filter isolates the spectral line of interest. The first polarizing cube transmits the horizontally polarized component of the filtered plasma light before traversing a birefringent crystal (typically $LiNbO_3$, $L = 25$ mm thick, birefringence $B = 0.1$) whose fast axis is at 45° to the plane of polarization. For light of centre frequency $\nu_0 = c/\lambda_0$, this introduces a phase delay $\phi_0 = 2\pi\nu_0 BL/c = 2\pi\nu_0\tau_0$ between the orthogonal characteristic waves. An additional small delay modulation $\tilde{\phi}_1 = 2\pi\nu_0\tilde{\tau}_1 = \phi_1 \sin(\Omega t)$ of amplitude $\phi_1 = \pi/2$ is imposed by applying an oscillating voltage (typically at tens of kilohertz) along the crystal z-axis. Finally, the light is once more polarized using a beamsplitter cube to allow the independent components to interfere at photomultiplier tubes intercepting the transmitted and reflected beams.

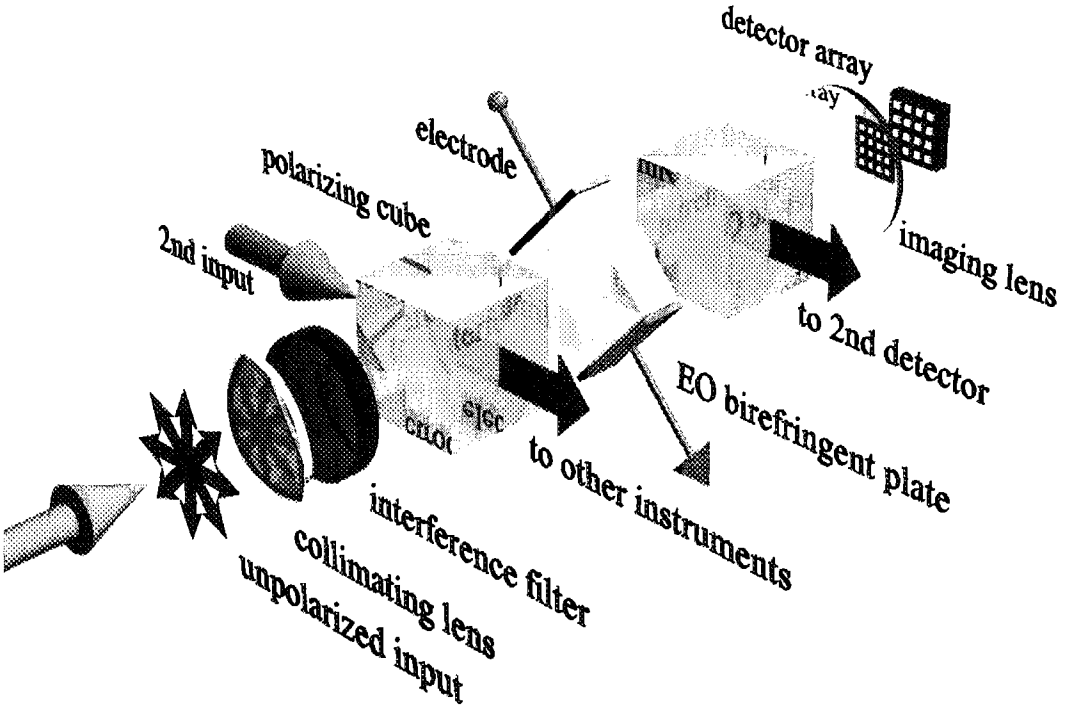

Figure 1: Optical layout for the modulated solid state spectrometer.

The operating principle of the instrument is illustrated in Fig. 2. When the species temperature increases (decreases), the light coherence decreases (increases). This is monitored by dithering the instrument phase electrooptically by $\pm\pi/2$ about the fixed delay (phase) offset. When the centre frequency changes,

the intereferogram expands or contracts and the offset phase changes. This is registered as a change in the ratio of the power in the odd and even harmonics of the applied modulation. Because of the large fixed delay τ_0, even small changes in wavelength can give significant shifts in the interferogram phase.

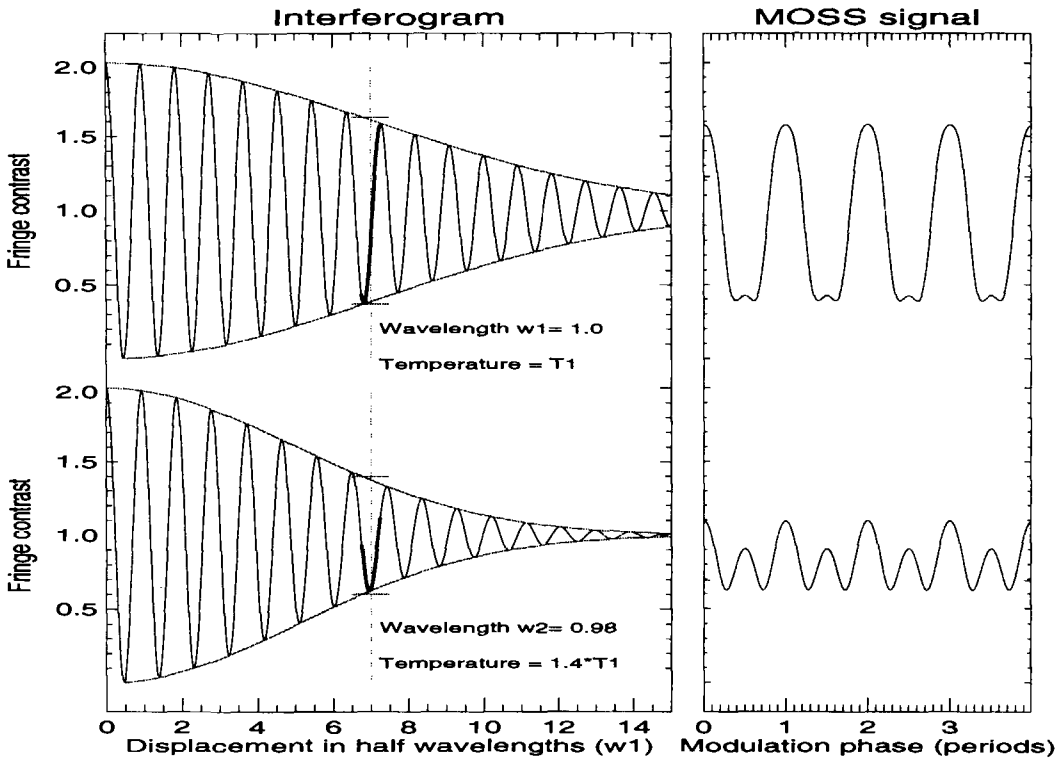

Figure 2: Simulated interferograms showing the effect on the interferogram phase of a change in line centre frequency (exaggerated for clarity). The dashed vertical line corresponds to the delay introduced by the birefringent crystal while the bold section is the portion of the interferogram swept by the electrooptic modulation. The fringe contrast also varies with changes in the temperature of the emitting species.

The intensity at the output port is proportional to

$$S_{\pm} = \int_0^{\infty} I(\nu, \hat{\boldsymbol{l}})[1 \pm \cos(\phi\nu/\nu_0)]\,\mathrm{d}\nu/\nu_0 \qquad (1)$$

where $\phi = \phi_0 + \tilde{\phi}_1$ is the total phase delay introduced by the birefringent crystal and $I(\nu, \hat{\boldsymbol{l}})$ is the line integrated intensity at impact parameter p on the plasma and in the direction $\hat{\boldsymbol{l}}$.

The high voltage modulation of the electrooptic plate(s) is achieved using a function generator, a standard audio-amplifier and step-up transformer (100:1).

This system has been optimized using a detailed circuit model (Cheetham, Michael and Howard - these proceedings) and is capable of operating over a range of frequencies from 0.5 kHz to 100kHz.

The low level signal to the modulator is provided by a PC card (PCI-MIO-16E-4) controlled using a LabVIEW virtual instrument. The card/software also acquires the MOSS signals, processes, displays and archives the data from up to 8 channels in real-time. Other instrumental issues such as sensitivity and resolution are discussed at length elsewhere [2].

3 Doppler Tomography

The most basic optical spectroscopy measures the Doppler shift and broadening of emission from excited plasma atoms and ions. Usually these measurements are line integrated. Though charge exchange recombination spectrosopy achieves a degree of localization, colder edge emission often masks the charge exchange light. Multi-channel measurements and tomographic techniques must then be employed. However, because of the summation of Doppler spectra of varying width and shift along the line-of-sight, spectral-domain (i.e. grating based) systems are not well suited for the inverse procedure.

We consider an inhomogeneous drifting isotropic velocity distribution function $f(\boldsymbol{r}, \boldsymbol{\beta} - \boldsymbol{\beta}_D)$ where $\boldsymbol{\beta}_D(\boldsymbol{r}) = \boldsymbol{v}_D/c$ is the normalized local drift velocity. The integrated measurement along some line L viewing the plasma in direction $\hat{\boldsymbol{l}}$ is given by

$$I(\xi; \hat{\boldsymbol{l}}) = \int_L I_0(\boldsymbol{r})\, g(\boldsymbol{r}, \xi; \hat{\boldsymbol{l}})\, \mathrm{d}l \tag{2}$$

where $\xi = (\nu - \nu_0)/\nu_0$ is a normalized optical frequency coordinate, $I_0(\boldsymbol{r})$ is the local emission spectrum and

$$g(\boldsymbol{r}, \xi; \hat{\boldsymbol{l}}) = \int f(\boldsymbol{r}, \boldsymbol{\beta} - \boldsymbol{\beta}_D)\, \delta(\xi - \boldsymbol{\beta}.\hat{\boldsymbol{l}})\, \mathrm{d}\boldsymbol{\beta}. \tag{3}$$

The delta function selects the part of the velocity distribution f that contributes via the Doppler effect to the optical intensity at normalized frequency ξ.

Taking the Fourier transform of Eq. (3) delivers a remarkable simplification – the contributions from the drift and the body of the distribution separate:

$$G(\boldsymbol{r}, \phi\hat{\boldsymbol{l}}) \equiv \mathcal{F}[g(\boldsymbol{r}, \xi; \hat{\boldsymbol{l}})] = \exp(\mathrm{i}\phi\boldsymbol{\beta}_D.\hat{\boldsymbol{l}})\hat{G}(\boldsymbol{r}, \phi\hat{\boldsymbol{l}}). \tag{4}$$

$\hat{G}(\boldsymbol{r}, \phi\hat{\boldsymbol{l}})$ is a central slice of the Fourier transform of $f(\boldsymbol{r}, \boldsymbol{\beta})$ in the direction $\hat{\boldsymbol{l}}$.

As noted above, this Fourier transform can be achieved optically using interferometric techniques. The MOSS spectrometer (interferometer) measures the complex coherence whose modulus (envelope) is independent of the spatially varying drift $\boldsymbol{\beta}_D$:

$$|\gamma(\phi; \hat{\boldsymbol{l}})| = \int_L I_0(\boldsymbol{r})\, \hat{G}(\boldsymbol{r}, \phi\hat{\boldsymbol{l}})\, \mathrm{d}l. \tag{5}$$

The inversion of Eq. (5) gives the isotropic but inhomogeneous distribution function $f(\boldsymbol{r}, \xi)$[4]. For a locally Maxwellian velocity distribution, this becomes:

$$|\gamma(\phi; \hat{\boldsymbol{l}})| = \int_L I_0(\boldsymbol{r}) \exp\left[-T_S(\boldsymbol{r})/T_C\right] \mathrm{d}l \tag{6}$$

where $T_S(\boldsymbol{r})$ is the species temperature distribution and T_C is a "characteristic temperature" set by the interferometer phase delay ϕ_0 and species mass m_S:

$$kT_C = \frac{1}{2} m_S v_C^2 \qquad\qquad v_C = \frac{2c}{\phi_0}. \tag{7}$$

Tomographic inversion of Eq. (6) gives $T_S(\boldsymbol{r})$.

The imaginary part (phase) of the interferogram is given (to first order in small quantities) by

$$\Im\left[\gamma(\phi; \hat{\boldsymbol{l}})\right] = \phi_0 \int_L I_0(\boldsymbol{r})\, \hat{G}(\boldsymbol{r}, \phi\hat{\boldsymbol{l}})\, \boldsymbol{\beta}_D . \mathrm{d}\boldsymbol{l} \tag{8}$$

where $\boldsymbol{l} = \hat{\boldsymbol{l}}\mathrm{d}l$. Observe that the small Doppler shift component is amplified by the fixed phase delay ϕ_0. Equation (8) is a vector field line integral whose inversion gives the vorticity of the field $I_0 \hat{G} \boldsymbol{\beta}_D$. Under conditions of LTE, we write $\hat{G} \equiv \zeta_S = \exp\left[-T_S(\boldsymbol{r})/T_C\right]$. Under some conditions, it is possible to reconstruct the component of the flow-field vector potential that is normal to the measurement plane [1].

4 MOSS Doppler measurements in H-1NF

If we ignore the spatial integration and assume LTE, Eq. (1) gives the signal at the spectrometer ports as

$$S_\pm = I_0 \pm I_0 \zeta \cos\left[\phi_0(1 + \beta_D) + \phi_1 \sin(\Omega t)\right] \tag{9}$$

where the total fringe visibility (coherence envelope) $\zeta = \zeta_I \zeta_S$ includes an instrumental component analogous to the familiar slit function for grating spectrometers. The instrumental fringe contrast ζ_I is determined by the collected light solid angle and optical imperfections, and can be represented by the factor $\zeta_I = \exp(-T_I/T_C)$, where T_I is the instrument "temperature". It is apparent that the source temperature T_S can be obtained from the measured fringe contrast via a simple subtraction of exponents proportional to the measured and instrumental temperatures rather than requiring the usual deconvolution correction for the instrument function.

Uncertainty in the instrumental phase offset ϕ_0 is equivalent to a wavelength calibration error for grating instruments. Generally, it is difficult to absolutely determine the phase shift ϕ_0 corresponding to a given wavelength ν_0. Estimates

of the Doppler drift β_D are usually obtained with respect to the measured phase ϕ_0 at the commencement of the discharge.

The unknown quantities I_0, β_D and T_S can be recovered numerically from $S_\pm$ synchronously sampled at times $t = 0, T/4, T/2, 3T/4, \ldots$ where $T = 2\pi/\Omega$ is the modulation period. The instrument is "optimum" in the sense that all available photons are used simultaneously to determine only the three unknown quantities I_0, β_D and T_S.

To demonstrate the instrument performance, we show temperature and flow data for an rf heated (7MHz, 80kW max) argon discharge in a low-shear magnetic configuration close to the 3/2 resonance. ArII light at 488nm is collected from a cylindrical plasma volume of diameter ~ 30 mm with axis parallel to the major axis of the bean-shaped plasma cross-section. The viewing chord can be translated across the plasma poloidal cross-section on a shot-to-shot basis. The system has been used for study of ion dynamics during confinement transitions and during power modulation experiments.

The observed ion temperatures are in the range 10-100 eV and match well the dynamic range for a $LiNbO_3$ crystal of thickness 25mm ($T_C = 70$ eV). The instrument temperature, measured using an expanded argon ion laser beam at 488nm is $\sim 20 - 25$ eV and arises from mainly imperfections in the birefringent plate. The estimated component due to beam divergence is less than a few eV.

By virtue of its high light throughput (in our case, ~ 40 times greater than for an equivalent-resolution grating instrument) and direct sensitivity to low order spectral moments, the MOSS spectrometer is especially well suited to measurements that require high time resolution such as for the observation of fluctuations and coherent modes.

Figure 3 shows the temporal evolution of various diagnostic signals for a discharge which exhibits a spontaneous transition from low to high confinement at $t = 13$ ms. The first two traces are the plasma line-density and stored energy. The MOSS quadrature sampled signal for a chord at position 20 mm outside the magnetic axis is the third signal (four independent traces are shown). The following three traces are the inferred zeroth moment $\langle I_0 \rangle$, ion temperature $\langle T_s \rangle$ and flow velocity $\langle v_D \rangle$, where angle brackets denote line-averaged quantities. Since the absolute phase for the unshifted spectral line is not calibrated, the absolute flow velocity is not significant. However, note that the change in flow velocity throughout the transition is small (< 500 m/s). This is also true at other measurement positions. The final trace is ArI atomic emission intensity showing a slight decrease at the time of the transition. The ion temperature has not been corrected for the instrument temperature, while the observed noise levels for the ion temperature and flow are consistent with estimates based on the light signal to noise ratio.

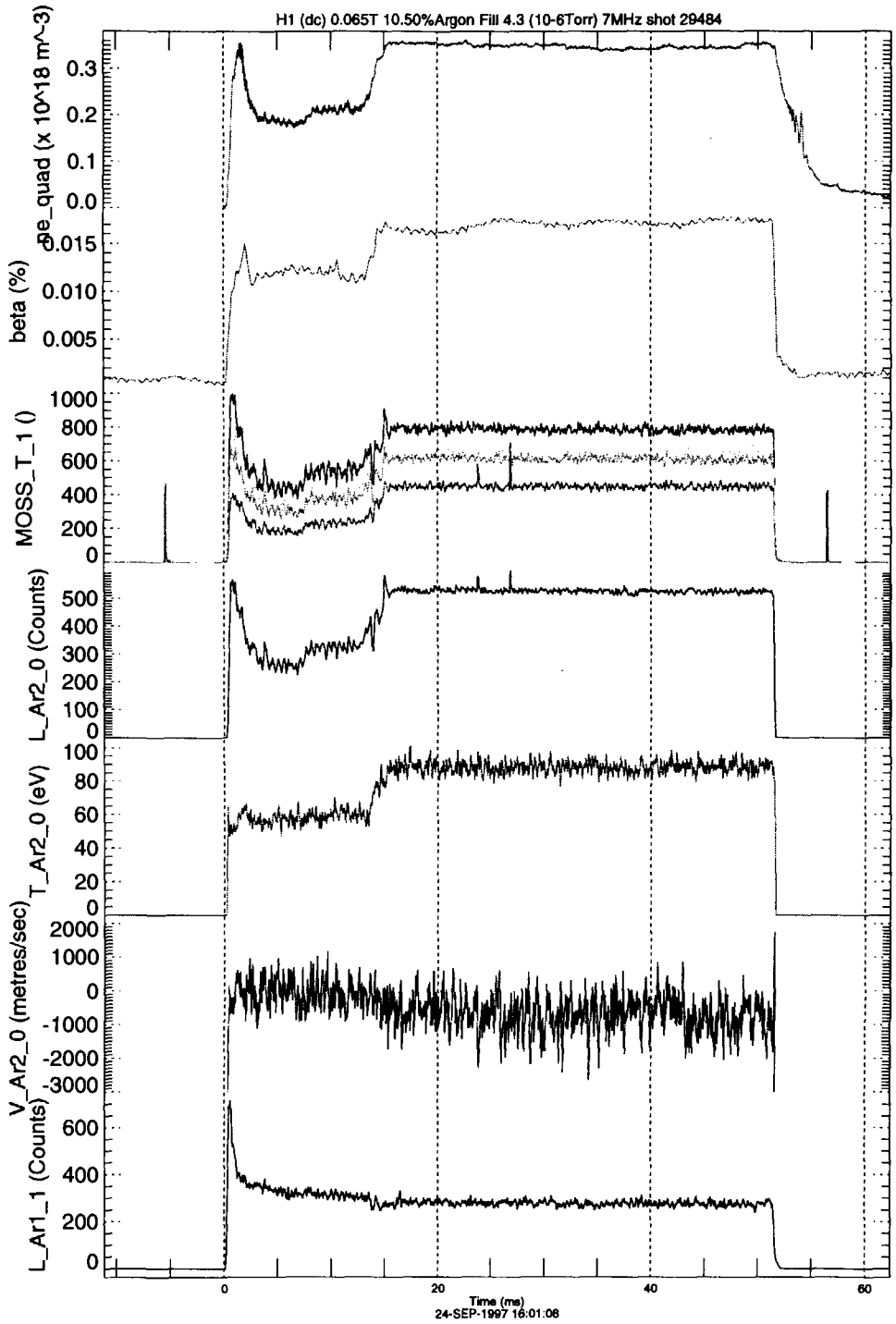

Figure 3: Plot showing temporal evolution of plasma parameters during spontaneous transition from low to high confinement at $t = 13$ ms. From top to bottom: Line averaged density, plasma stored energy, quadrature sampled MOSS light signal at impact parameter -20 mm , inferred light intensity, ion temperature, flow velocity and ArI atom light emission intensity.

4.1 Spectroscopic Camera

It is natural to extend the MOSS spectrometer to allow for multiple spatial channels. Because the information is contained in the temporal frequency domain, it is possible to use the camera for truly two-dimensional plasma spectral imaging with high time-resolution. Each spatial channel requires its own detector, and the associated signals must be separately acquired. Commercially available multi-anode photomultiplier detectors (MAD) are well suited for this application. We are constructing two cameras. One views the plasma directly using a 16 element linear detector array (Michael and Howard - these proceedings). The second camera utilizes an 8 $\times$ 8 MAD array to process light input from an array of 55 lens-coupled optical fibres as described below. Issues such as instrument contrast and field-of-view are discussed in the companion paper by Michael and Howard.

4.2 ToMOSS

The Tomographic MOSS (ToMOSS) spectroscopy experiment is designed to obtain detailed tomographic reconstructions of edge flow fields and temperature distributions in the H-1 heliac. A large diameter ($\sim$ 800mm) rotatable stainless steel ring that encircles the plasma in a poloidal cross-section, is used for mounting 5 independent modules each containing 11 lens coupled optical fibres for collecting plasma light emission along parallel chords separated by $\sim$ 20mm. Fig. 4 shows the mounting ring, supporting frame and the five sets of viewing chords superimposed on the plasma cross-section. A photograph of one of the optical modules showing the collecting lenses is given in Fig 5.

The optical fibres drape around the edge of the wheel and are shielded from the plasma. The lenses can be rotated away from the plasma region when not in use. An array of narrow (4mm) fluorescent tubes are located in the viewing cross-section (above the plasma region) for calibrating the relative channel sensitivities. The fibres exit the H-1 vacuum chamber via rubber O-ring seals and terminate at a patch panel. The rotatble ring, which has been recently installed, is driven by a stepper motor outside the vacuum vessel under CAMAC control. Light from the 55 channels will be fibre coupled to an imaging MOSS camera and the parallel signals acquired via CAMAC.

4.3 Spread-spectrum methods - the SOFT spectrometer

A generalization of the MOSS spectrometer that utilizes a number of birefringent electrooptic plates mutually aligned at 45° and placed between crossed or parallel polarizers has been constructed and tested. The Spread-spectrum Optical Fourier Transform (SOFT) Spectrometer allows simultaneous measurements of the coherence enevlope of a narrowband spectral feature at a multiplicity of

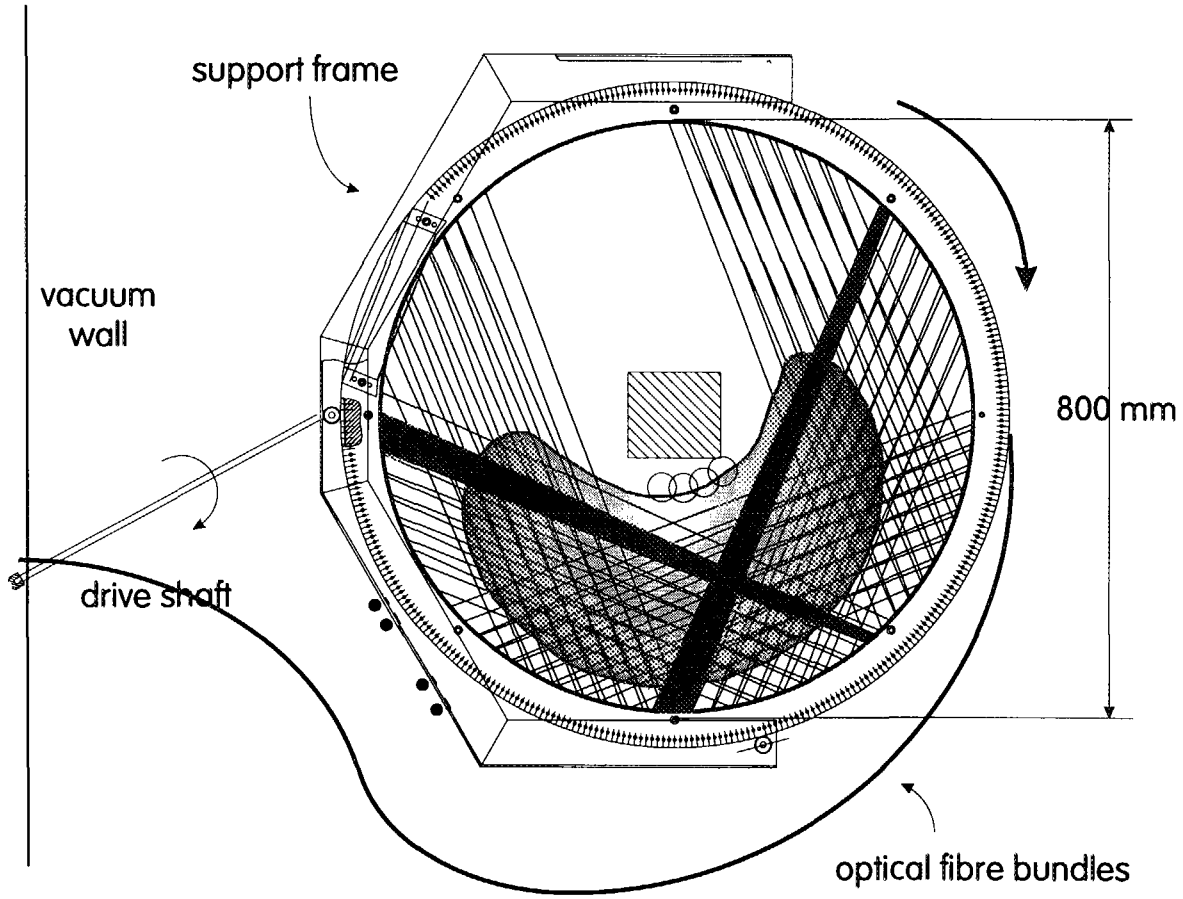

Figure 4: Schematic drawing of ToMOSS optical ring and support structure showing plasma region and viewing chords. Two chords have been shaded for clarity.

delays. As its name suggests, the information is now encoded across a series of harmonics of the common sinusoidal drive voltage applied to the electrooptic crystals.

A representative 3-crystal layout for the SOFT spectrometer is shown in Fig. 6. The three crystals give rise to six independent fixed delay modulated interferometers. Because the modulation indices ϕ_{1i} are in the same ratio as the delays ϕ_{0i}, the larger the delay, the greater is the modulation depth and the higher in frequency are the generated harmonic carriers.

The interferogram can be processed numerically using a series of bandpass filters centred on the respective carriers and having a bandwidth determined by

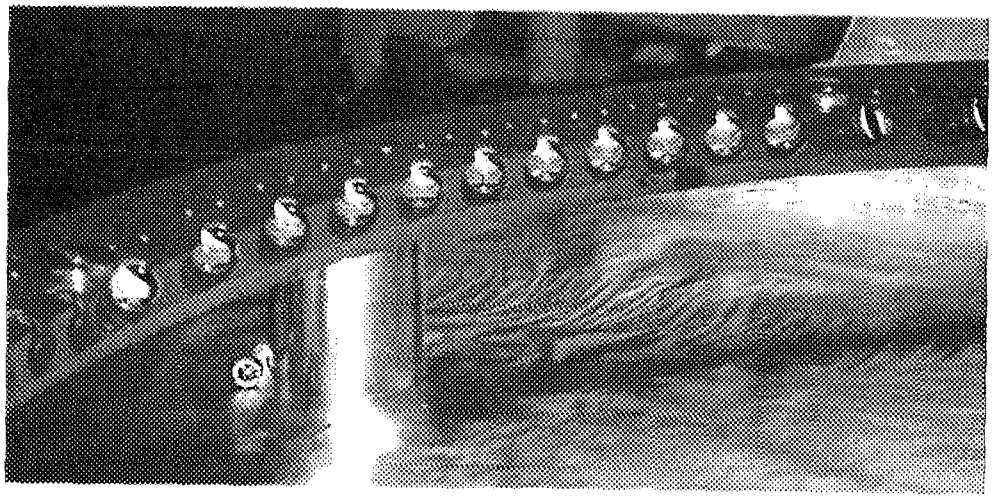

Figure 5: Photograph of lens-coupled fibre module. The lenses are 5mm in diameter. Five such modules are mounted on the carrier ring at intervals of 45°.

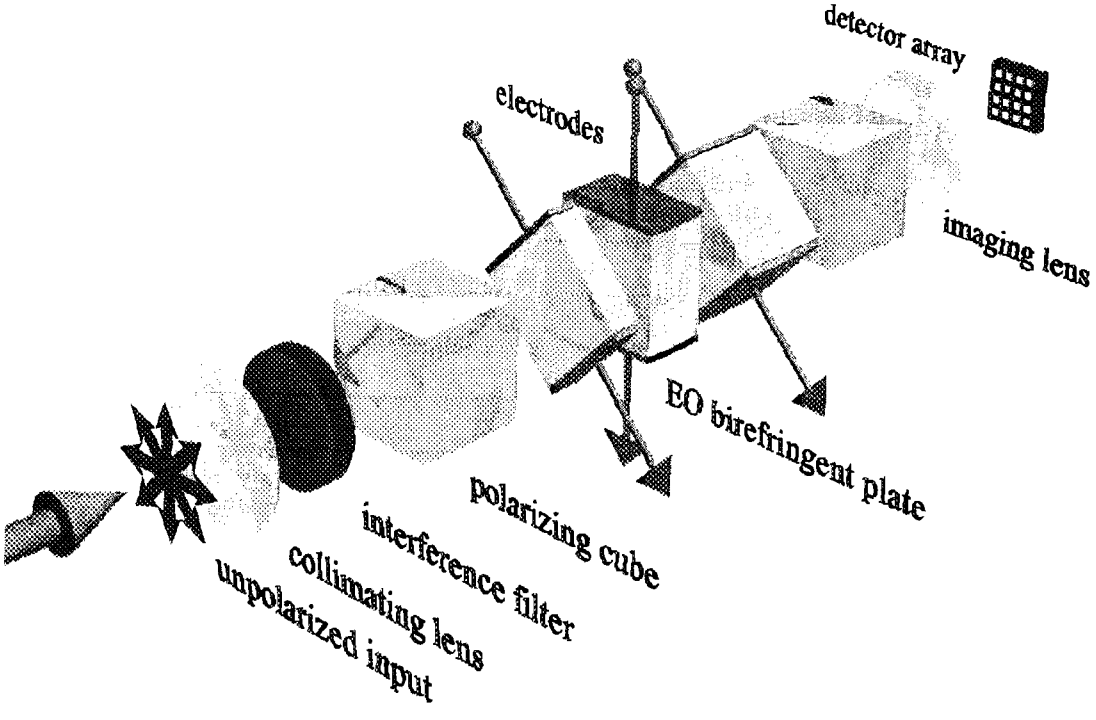

Figure 6: Diagram showing the relative orientation of the polarizers and birefringent crystals for a 3-crystal SOFT spectrometer.

the plasma properties and the modulation frequency. Inverse FFT recovers a set of time vectors which can be unwrapped to extract 12 independent pieces of information pertaining to the spectral line shape. The drive voltage should be sufficient to produce a modulation amplitude of at least $\pi/2$ radians for the interferometer having the least phase delay offset to ensure data inversion with good condition number. The SOFT spectrometer is ideal for the study of non-thermal or complex spectra or for effectively extending the dynamic range of the MOSS spectrometer.

Acknowledgements

It is a pleasure to acknowledge technical assistance provided by Mr J. Wach, Mr M. Blacksell and Mr. Rob Davies.

References

[1] J. HOWARD. Vector tomography applications in plasma diagnostics. *Plasma Phys. Control Fusion*, 38:489–503, 1996.

[2] J. HOWARD. Electro-optically modulated solid state spectrometer for plasma flow and temperature diagnostics. *Rev. Sci. Instrum.*, page In Preparation, 1999.

[3] J. HOWARD. Modulated optical solid-state spectrometer applications in plasma diagnostics. *Rev. Sci. Instrum.*, 70:368–371, 1999.

[4] J. HOWARD. Doppler spectroscopy of extended radiating media. *J. Opt. Soc. Am. A*, 1999 (submitted).